Earth and Planetary Science Letters 465 (2017) 29–37

Contents lists available at ScienceDirect

Earth and Planetary Science Letters

www.elsevier.com/locate/epsl

Thermal conductivity of ferropericlase in the Earth's lower mantle

Kenji Ohta [a,*], Takashi Yagi [b], Kei Hirose [c], Yasuo Ohishi [d]

[a] Department of Earth and Planetary Sciences, Tokyo Institute of Technology, Ookayama, Meguro, Tokyo 152-8551, Japan
[b] National Metrology Institute of Japan, National Institute of Advanced Industrial Science and Technology, Ibaraki 305-8563, Japan
[c] Earth-Life Science Institute, Tokyo Institute of Technology, Tokyo 152-8550, Japan
[d] Japan Synchrotron Radiation Research Institute, Hyogo 679-5198, Japan

ARTICLE INFO

Article history:
Received 27 October 2016
Received in revised form 17 January 2017
Accepted 18 February 2017
Available online 7 March 2017
Editor: J. Brodholt

Keywords:
(Mg, Fe)O ferropericlase
thermal conductivity
electrical conductivity
spin crossover
core–mantle boundary heat flow

ABSTRACT

(Mg, Fe)O ferropericlase (Fp) is one of the important minerals comprising Earth's lower mantle, and its thermal conductivity could be strongly influenced by the iron content and its spin state. We examined the lattice thermal conductivity of (Mg, Fe)O Fp containing 19 mol% iron up to 111 GPa and 300 K by means of the pulsed light heating thermoreflectance technique in a diamond anvil cell. We confirmed a strong reduction in the lattice thermal conductivity of Fp due to iron substitution as reported in previous studies. Our results also show that iron spin crossover in Fp reduces its lattice thermal conductivity as well as its radiative conduction. We also measured the electrical conductivity of an identical Fp sample up to 140 GPa and 2730 K, and found that Fp remained an insulator throughout the experimental conditions, indicating the electronic thermal conduction in Fp is negligible. Because of the effects of strong iron impurity scattering and spin crossover, the total thermal conductivity of Fp at the core–mantle boundary conditions is much smaller than that of bridgmanite (Bdg). Our findings indicate that Bdg (and post-perovskite) is the best heat conductor in the Earth's lower mantle, and distribution of iron and its valence state among the lower mantle minerals are key factors to control the lower mantle thermal conductivity.

1. Introduction

The core–mantle boundary (CMB) is by far the most important thermal boundary layer inside the Earth, and the heat flow through the CMB largely controls the thermal structure and evolution of the Earth's interior (see a review by Lay et al., 2008). Since the heat across the boundary is only transported by conduction, understanding terrestrial heat transport requires knowledge of thermal conductivity of the mantle-forming minerals as functions of pressure, temperature, and chemical composition. In addition, the lowermost mantle is considered to be thermally and chemically heterogeneous, leading to heterogeneous thermal conductivity and heat flux at the base of the mantle (Ammann et al., 2014; Stackhouse et al., 2015). The spatial variation in the CMB heat flux potentially influences 1) the outer core convection and thus the pattern, strength, and evolution of the Earth's magnetic field, 2) the structure and age of the inner core (Sumita and Olson, 1999; Olson, 2016), and 3) small-scale mantle convection style (Ammann et al., 2014). Recent estimates of the lowermost mantle thermal conductivity span a wide range from 4 to 21 W/m/K, which is mainly due to ill-constrained temperature and compositional effects (Kavner and Rainey, 2016).

The thermal conductivity of a material is estimated by the sum of lattice, radiative, and electronic thermal conductivities. Lattice thermal conduction occurs by phonon–phonon scattering and is likely the primary form of thermal conductivity at the Earth's mantle conditions (Hofmeister, 1999). Heat also moves diffusively by photons at high temperature, which may play an important role at conditions relevant to the Earth's lowermost mantle. Electronic thermal conduction is most considerable in metallic material among these three conduction mechanisms.

Ferropericlase (Fp) is the second most abundant mineral in the Earth's lower mantle after (Fe, Al)-bearing $MgSiO_3$ bridgmanite (Bdg). The lower mantle Fp contains approximately 20% ferrous iron in the octahedral site of the cubic rock-salt crystal structure (e.g., Sinmyo et al., 2008). MgO periclase, the endmember of (Mg, Fe)O, has often been used to estimate the thermal conductivity of the lower mantle. Thus, extensive data exists on the thermal conductivity (or thermal diffusivity) of MgO at high pressures (P) and temperatures (T) (Touloukian et al., 1970; de Koker, 2010; Stackhouse et al., 2010; Tang and Dong, 2010; Manthilake et al., 2011; Haigis et al., 2012; Dalton et al., 2013; Imada et al., 2014). Pure crystals with higher symmetry exhibit relatively small phonon–phonon interaction, hence a high thermal conductivity. In-

* Corresponding author.
E-mail address: k-ohta@geo.titech.ac.jp (K. Ohta).

http://dx.doi.org/10.1016/j.epsl.2017.02.030
0012-821X/

deed, MgO periclase is one of the best heat conductors among rock-forming minerals of the Earth's mantle (Hofmeister, 1999). However, the iron impurity in Fp acts as an additional phonon scatterer and could weaken its lattice thermal conduction significantly. Existing reports demonstrated a large degree of reduction in the conductivity due to iron substitution (Morton and Lewis, 1971; Manthilake et al., 2011; Tang et al., 2014; Goncharov et al., 2015). However, the lattice thermal conductivity ($\kappa_{\rm latt}$) of Fp with a realistic mantle composition (~20 mol% FeO) remains to be determined at high pressures up to 14 GPa (Manthilake et al., 2011).

The key feature of (Mg, Fe)O Fp in the Earth's deep mantle is the occurrence of iron spin crossover. This changes its thermoelastic, rheological, and transport properties (see Lin et al., 2013 for a review). Iron partitioning between Fp and Bdg also changes upon the spin crossover (Irifune et al., 2010). It has been reported that the change in the optical absorption property of Fp across the spin crossover induces the reduction in its radiative thermal conductivity ($\kappa_{\rm rad}$) (Goncharov et al., 2006; Keppler et al., 2007). On the other hand, Stackhouse et al. (2015) speculated that, based on scaling relations, the $\kappa_{\rm latt}$ of Fp might be about 3% higher in the low-spin state than in the high-spin state. However, the $\kappa_{\rm latt}$ of Fp in the low-spin state has not been measured yet. In addition, the electronic density of state calculations by Holmström and Stixrude (2015) showed an insulator–metal transition in $(Mg_{0.75}Fe_{0.25})O$ Fp at lower mantle conditions, suggesting not important $\kappa_{\rm rad}$ of low-spin Fp. Their Kubo–Greenwood computations gave the electronic component of the electrical conductivity ($\sigma_{\rm el}$) of $(Mg_{0.75}Fe_{0.25})O$ Fp as $4.0(\pm 0.4) \times 10^4$ S/m at the CMB conditions. This value corresponds to 3.6 ± 0.4 W/m/K of electronic thermal conductivity ($\kappa_{\rm el}$) when using the Wiedemann–Franz relation;

$$\kappa_{\rm el} = \sigma_{\rm el} T L_0, \tag{1}$$

where T is absolute temperature, and L_0 is the Sommerfeld value of the Lorenz number (2.445×10^{-8} W Ω/K^2). However, no experimental confirmation of such enhanced $\kappa_{\rm el}$ and $\sigma_{\rm el}$ of Fp at the deep lower mantle conditions has been made so far. To determine the total thermal conductivity of Fp, direct measurements of $\kappa_{\rm latt}$ and $\sigma_{\rm el}$ are required.

In this letter, we report the results of $\kappa_{\rm latt}$ measurements on $(Mg_{0.81}Fe_{0.19})O$ Fp up to 111 GPa and 300 K. Iron content of the sample likely represents that of Fp in the Earth's lower mantle (e.g., Sinmyo et al., 2008). Our experiments aim to clarify the compositional dependence of $\kappa_{\rm latt}$ in the MgO–FeO solid solution, and the effect of spin crossover on $\kappa_{\rm latt}$ at high P–T conditions. We also performed *in-situ* high P–T electrical conductivity measurements on $(Mg_{0.81}Fe_{0.19})O$ Fp to verify the possible enhancement of electronic conduction with elevating pressure and temperature. On the basis of our experimental results, we estimate the thermal conductivity of the lower mantle at the CMB, and discuss its consequences on the dynamics of the core and the mantle.

2. Experimental procedure

2.1. Sample characterization and high-pressure generation

The sample is a polycrystalline $(Mg_{0.81}Fe_{0.19})O$ Fp, which was synthesized at 1.2 GPa and 1570 K for 19 hrs in a piston cylinder apparatus at the Tokyo Institute of Technology. Talc-Pyrex outer sleeve and graphite furnace were used. $Fe^{3+}/(Fe^{2+} + Fe^{3+})$ ratio in our sample was estimated to be 0.049 ± 0.017 from $d_{220} = 1.49787 \pm 0.00007$ Å and the total iron content of our Fp sample according to the method by Dobson et al. (1998). Such small amount of Fe^{3+} (i.e., point defects) is unlikely to have significant effect on the $\kappa_{\rm latt}$ of Fp. Pressure–volume–temperature (P–V–T) equation of state (EOS) of Fp with same chemical compositions have been proposed (Komabayashi et al., 2010). The spin crossover in $(Mg_{0.81}Fe_{0.19})O$ Fp occurs between ~30 and ~55 GPa at room temperature, based on previous compression experiments and *ab initio* calculations (Tsuchiya et al., 2006; Komabayashi et al., 2010).

High-pressure conditions were generated in a diamond anvil cell (DAC) with 300, 150 or 120 μm culet diamond anvils. The pressure was determined from the wavelength of ruby fluorescence and from the Raman shift of the diamond anvil (Akahama and Kawamura, 2006) in the experiments for $\kappa_{\rm latt}$ determination. In the case of electrical conductivity measurements, pressure was calibrated from the unit-cell volume of gold electrodes based on the EOS of gold (Tsuchiya, 2003).

2.2. Lattice thermal conductivity measurement

We employed the pulsed light heating thermoreflectance technique for high-pressure lattice thermal diffusivity measurement in a DAC (Yagi et al., 2011). The Fp sample, coated with sputtered Au film, was loaded into a sample chamber in a rhenium gasket together with a sapphire single crystal disk and KCl, which served the sample as a pressure transmitting media and thermal insulator against diamond anvils. Heating was made on the sample surface using a pulsed YAG laser with pulse duration of 2 ns and pulse energy of 0.5 μJ. A linearly polarized continuous-wave diode laser (532 nm in wavelength) was focused on the opposite side of the Au film to measure the rise in temperature using the thermoreflectance effects of gold. The Au foils covering the sample acted as a laser absorber on the side heated by pump laser, and as laser reflector (temperature sensor) on the probe laser side. A high-speed photo detector monitored the intensity of the reflected probe laser, and the measured signal was averaged in an oscilloscope (500 MHz in bandwidth). The transient temperature change was recorded at high pressures as shown in Fig. 1a. Details of the measurement technique have been described previously (Yagi et al., 2011; Ohta et al., 2012a). Prior to each thermoreflectance measurement, we carried out laser annealing to release deviatoric stress in the sample chamber.

After the high-pressure thermoreflectance measurement, the thickness of both Fp and Au films was measured in a sample recovered from the DAC. Its cross section was prepared by using the focused ion beam (FIB) apparatus, and the thickness of Fp and Au foils was obtained under a scanning electron microscope (SEM). Then we estimated their thickness at high pressure based on the reported P–V–T EOSs of $(Mg_{0.81}Fe_{0.19})O$ Fp and Au, assuming elastic deformation (Tsuchiya, 2003; Komabayashi et al., 2010).

The obtained temperature history curves were analyzed considering the one-dimensional heat diffusion in Fp, Au foils, and the pressure medium:

$$T(t) = \overline{T}\sqrt{\frac{\tau}{\pi t}}\sum_{n=0}^{\infty}\gamma^{2n}\exp\left[-\frac{(2n+1)^2}{4}\frac{\tau}{t}\right], \tag{2}$$

where $T(t)$ is temperature, $\overline{T}$ is a constant, t is time, and γ expresses heat effusion to pressure medium (Yagi et al., 2011). τ is heat diffusion time across the Fp sample and the Au foil. We obtained $\overline{T}$, γ and τ by fitting the measured curves to Eq. (2) as shown in Fig. 1b, c. Subsequently, τ was analyzed to acquire thermal diffusivity of ferropericlase ($D_{\rm Fp}$) based on the three-layer model of Au/Fp/Au using the following equations:

$$D_{\rm Fp} = \frac{(\frac{\Gamma}{6}) + 1 + (\frac{1}{\Gamma})}{(\Gamma+2)(\frac{\tau}{6}) - (\Gamma+\frac{4}{3})(\frac{d_{\rm Au}^2}{D_{\rm Au}})} d_{\rm Fp}^2 \tag{3}$$

$$\Gamma = \frac{C_{\rm Fp} d_{\rm Fp}}{C_{\rm Au} d_{\rm Au}}, \tag{4}$$

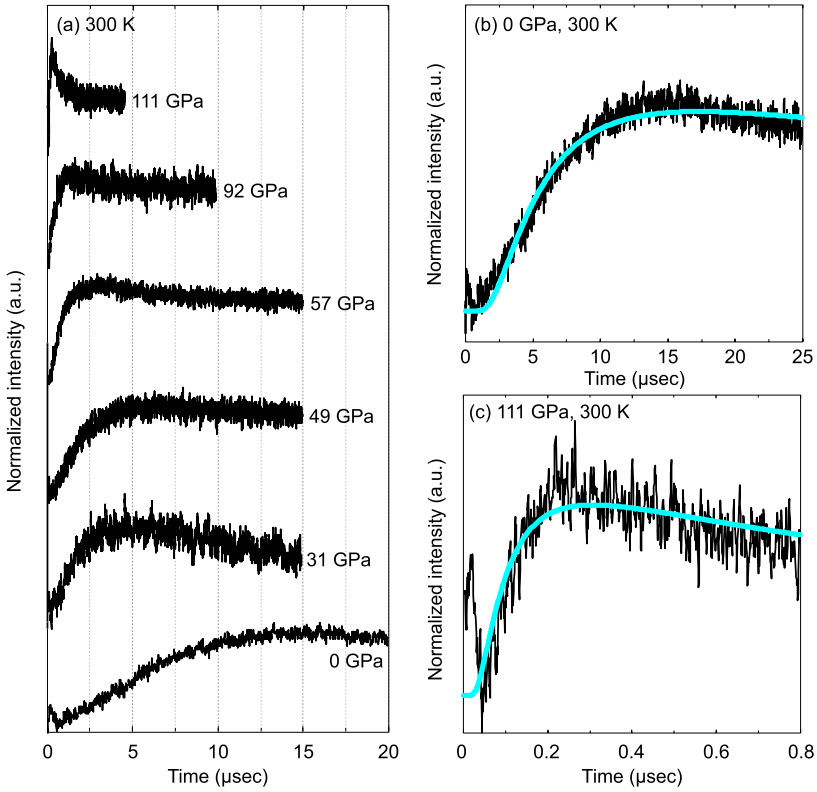

Fig. 1. (a) Transient temperature curves obtained at room temperature and high pressures of 0, 31, 49, 57, 92, and 111 GPa. Results of fitting to the transient temperature curves obtained at (b) 0 GPa and (c) 111 GPa by Eq. (2) (light blue curves). (For interpretation of the references to color in this figure legend, the reader is referred to the web version of this article.)

where D represents thermal diffusivity and C is heat capacity per unit volume ($C = \rho C_P$). D_{Au} is known to be 127 mm^2/s at ambient conditions with pressure derivative of 4%/GPa (Ho et al., 1972; Ross et al., 1984). The density (ρ) and heat capacity at constant pressure (C_P) of Au were from Tsuchiya (2003). The ρ of $(Mg_{0.81}Fe_{0.19})O$ Fp at each pressure was calculated from its EOS (Komabayashi et al., 2010). We calculated C_P of Fp at high pressures from its thermoelastic parameters (Speziale et al., 2007) on the basis of the Debye model and thermodynamic functions. We finally determined the κ_{latt} of Fp at high pressures from the multiplication of D_{Fp} and C_{Fp}.

The uncertainty in the obtained lattice thermal diffusivity (u_D) can be estimated from the following equation:

$$u_D = \sqrt{\left(\frac{\partial D}{\partial d}\right)^2 u_d^2 + \left(\frac{\partial D}{\partial \tau}\right)^2 u_\tau^2} = \sqrt{(2u_d)^2 + (u_\tau)^2}, \quad (5)$$

where $(\frac{\partial D}{\partial d})$ and $(\frac{\partial D}{\partial \tau})$ are sensitivity coefficients, and u_d and u_τ are uncertainties in sample thickness and heat diffusion time, respectively.

2.3. Electrical conductivity measurement

We performed electrical resistance measurements of $(Mg_{0.81}Fe_{0.19})O$ Fp at high P–T using a quasi-four-terminal method, concurrently with *in-situ* X-ray diffraction (XRD) measurements at BL10XU, SPring-8. The disk of Fp sample and the Au electrodes were sandwiched between Al_2O_3 layers in a sample chamber at the center of the electrically insulating cBN + rhenium composite gasket. The sample was heated in a double-sided heating system with a couple of fiber lasers. These procedures are the same as those employed in our previous studies for $Fe_{0.96}O$ wüstite and (Mg, Fe)O magnesiowüstite (Ohta et al., 2012b, 2014a). The electrical conductivity of Fp was estimated from the obtained electrical resistance and the sample geometry that is defined by the distance between electrodes, the size of a laser spot, and the thickness of the sample. Each measurement was carried out after thermal annealing that reduced deviatoric stress in the sample.

3. Results and discussion

3.1. Lattice thermal conductivity of $(Mg_{0.81}Fe_{0.19})O$ Fp up to 111 GPa

We performed 16 separate experiments to obtain the κ_{latt} of $(Mg_{0.81}Fe_{0.19})O$ Fp from 1 bar to 111 GPa at 300 K (Table 1). At ambient conditions, the κ_{latt} of MgO, $(Mg_{0.90}Fe_{0.10})O$, and $Fe_{1-x}O$ were reported to be 55, 5.7 and 5 W/m/K, respectively (Touloukian et al., 1970; Akiyama et al., 1992; Goncharov et al., 2015). Morton and Lewis (1971) also reported that the κ_{latt} of MgO with 3000 and 7500 ppm FeO are 48 and 31 W/m/K, respectively. We determined the κ_{latt} of $(Mg_{0.81}Fe_{0.19})O$ Fp to be 4.2 ± 0.5 W/m/K, in good agreement with previous reports (Touloukian et al., 1970; Morton and Lewis, 1971; Akiyama et al., 1992; Goncharov et al., 2015). As expected, our result confirms iron substitution in MgO notably weakens the lattice thermal conduction.

Fig. 2 shows the pressure response of the κ_{latt} of $(Mg_{0.81}Fe_{0.19})O$ Fp at 300 K plotted together with the values for MgO and $(Mg_{0.90}Fe_{0.10})O$ (Dalton et al., 2013; Goncharov et al., 2015). The κ_{latt} increased from 4.2 ± 0.5 W/m/K at 1 bar to 7.4 ± 2.3 W/m/K at 31 GPa. Then, it began to decrease and reached a minimum value of 4.0 ± 0.8 W/m/K at 37 GPa. The κ_{latt} then increased again, but showed weaker pressure dependence than that below 31 GPa. The value of κ_{latt} at 111 GPa is 15.2 ± 4.2 W/m/K, which is a factor of 3.6 higher than that at ambient conditions. Such an anomalous pressure response was not observed for MgO periclase (Dalton et al., 2013; Imada et al., 2014), and is most likely caused by the iron spin crossover in Fp (discussed in Section 3.3).

Table 1
Experimental pressures, spin state, and thermal diffusivity and conductivity of $(Mg_{0.81}Fe_{0.19})O$ ferropericlase.

Run #	Pressure (GPa)	Spin state	Thermal diffusion time (μs)	Thickness[a] (μm)	Thermal diffusivity (mm^2/s)	Thermal conductivity (W/m/K)
1	0	high	34.60(23)	5.88(31)	1.15(13)	4.19(47)
2	6.7	high	12.60(10)	4.24(35)	1.55(27)	5.75(101)
3	12.4	high	17.30(8)	5.34(22)	1.80(16)	6.74(60)
4	18.3	high	5.84(11)	3.36(34)	2.32(51)	8.84(193)
5	24.8	high	2.85(3)	2.10(25)	1.98(49)	7.59(190)
6	29.6	high	5.00(8)	2.56(28)	1.46(34)	5.64(131)
7	31.0	high	8.93(31)	4.00(54)	1.92(58)	7.43(225)
8	36.5	mix	3.02(8)	1.56(13)	1.01(19)	3.95(76)
9	41.9	mix	14.20(19)	3.79(32)	1.17(21)	4.65(85)
10	48.5	mix	11.10(15)	3.94(53)	1.50(42)	6.47(182)
11	56.5	mix	4.63(6)	2.43(34)	1.54(45)	6.26(181)
12	58.8	low	8.75(5)	3.91(53)	1.88(51)	7.64(209)
13	65.3	low	3.57(15)	2.49(27)	1.94(50)	7.92(206)
14	81.1	low	0.70(3)	1.44(16)	3.27(94)	13.54(388)
15	91.5	low	2.10(7)	2.07(13)	2.31(37)	9.64(156)
16	111.0	low	0.61(2)	1.42(17)	3.61(99)	15.20(416)

[a] After correction for pressure effect using P–V–T equation of $(Mg_{0.81}Fe_{0.19})O$ (Komabayashi et al., 2010).

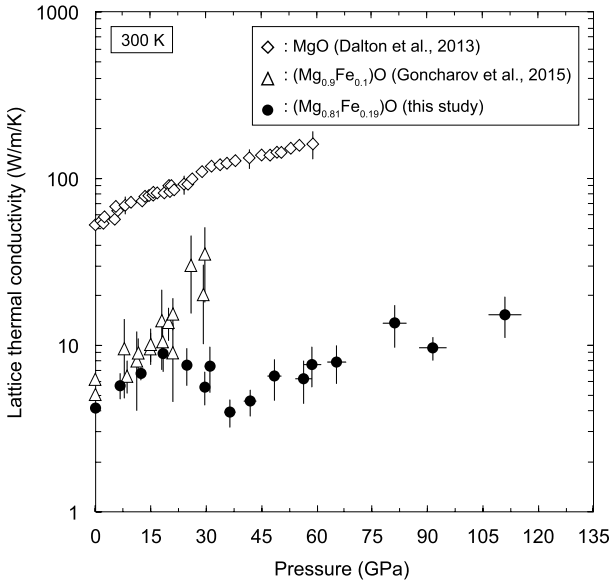

Fig. 2. κ_{latt} of (Mg, Fe)O as a function of pressure at 300 K. Solid circles, $(Mg_{0.81}Fe_{0.19})O$ (this study); triangles, $(Mg_{0.9}Fe_{0.1})O$ (Goncharov et al., 2015); diamonds, MgO (Dalton et al., 2013).

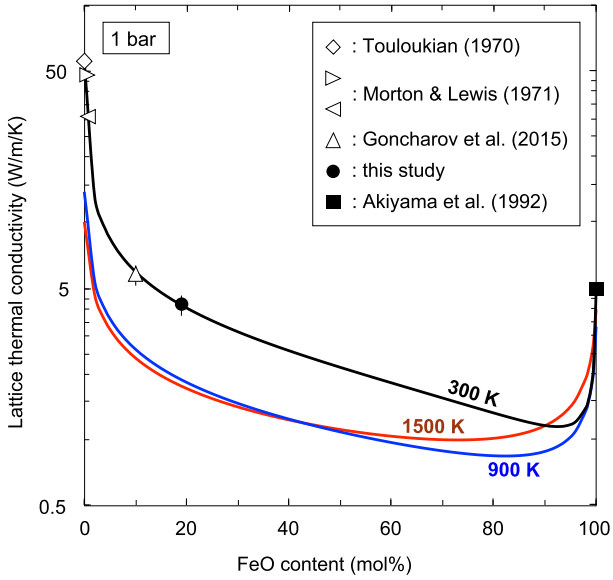

Fig. 3. Experimentally measured κ_{latt} of (Mg, Fe)O as a function of FeO content at 1 bar and different temperatures. Diamond, MgO (Touloukian et al., 1970); right and left-pointing triangles, MgO with 3000 ppm Fe and 7500 ppm Fe, respectively (Morton and Lewis, 1971); triangle, $(Mg_{0.9}Fe_{0.1})O$ (Goncharov et al., 2015); circle, $(Mg_{0.81}Fe_{0.19})O$ (this study); square, $Fe_{1-x}O$ (Akiyama et al., 1992). Eq. (7) is represented by solid curves for $T = 300$ K (black), 900 K (blue), and 1500 K (red). (For interpretation of the references to color in this figure legend, the reader is referred to the web version of this article.)

In this study, we used a polycrystalline Fp sample in which the effect of grain boundary scattering is important for κ_{latt} when the phonon mean free path is similar to the grain size. The effect of grain boundary scattering can be evaluated from the following equation:

$$\kappa_{poly}^{-1} = \kappa_{single}^{-1} + nR_{GB}, \tag{6}$$

in which κ_{poly}, κ_{single}, n, and R_{GB} indicate the thermal conductivities of polycrystalline and single crystal, the number of grain boundaries per meter along heat flow, and the grain boundary thermal resistance, respectively (Smith et al., 2003). Using FIB-SEM apparatus, we confirmed that a typical grain in our Fp sample is $0.5 \sim 4$ μm in size after the high-pressure experiment, which indicates that n is about 5.0×10^5 m^{-1}. We assumed R_{GB} of Fp is the same as that of alumina and periclase which is 1.0×10^{-8} m^2K/W (Smith et al., 2003; Imada et al., 2014). Combined with the present κ_{poly} of $(Mg_{0.81}Fe_{0.19})O$ Fp at 1 bar, Eq. (6) predicts that κ_{single} of Fp shows 2% higher value than κ_{poly}. In case of our data at 111 GPa, 10% underestimate against κ_{single} of Fp may exist. However, the estimated grain boundary effect for Fp is much smaller than that for MgO periclase (Imada et al., 2014), and is within the experimental uncertainty in the obtained κ_{latt} (Table 1). The mean free path of the phonon in Fp could be much shorter than that of MgO periclase due to strong iron impurity scattering, and thus the κ_{latt} of Fp (and also magnesiowüstite) should be insensitive to the grain size relative to that of MgO periclase.

3.2. Lattice thermal conductivity in the MgO–FeO system at 1 bar

Here we model the iron impurity effect on the κ_{latt} of the MgO–FeO solid solution by combining the present result with literature data (Touloukian et al., 1970; Morton and Lewis, 1971; Akiyama et al., 1992; Goncharov et al., 2015) (Fig. 3). Padture and Klemens (1997) proposed a model that predicts the effect of scattering by solute atom on the κ_{latt}:

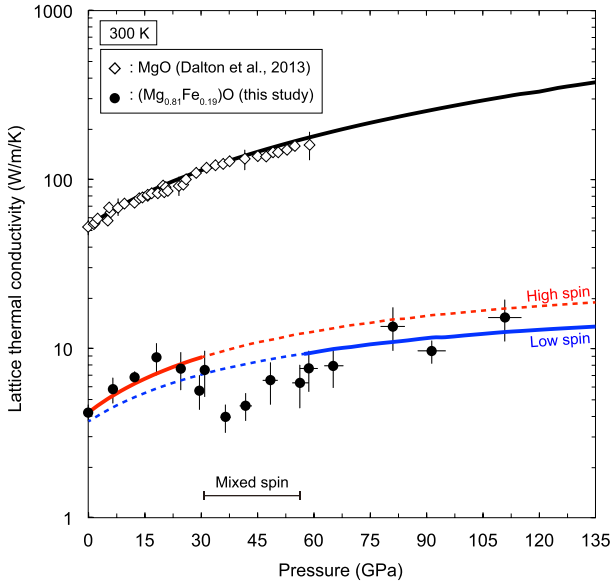

Fig. 4. Change in κ_{latt} of MgO periclase and $(Mg_{0.81}Fe_{0.19})O$ Fp with increasing pressure at 300 K. Diamonds, MgO (Dalton et al., 2013); circles, $(Mg_{0.81}Fe_{0.19})O$ (this study). Black, red, and blue lines indicate the pressure dependence of lattice thermal conductivities of MgO, high-spin $(Mg_{0.81}Fe_{0.19})O$, and low-spin $(Mg_{0.81}Fe_{0.19})O$ based on the damped harmonic oscillator–phonon gas model (Hofmeister, 1999) with reported thermoelastic properties of these minerals (Speziale et al., 2007; Tange et al., 2009). (For interpretation of the references to color in this figure legend, the reader is referred to the web version of this article.)

$$\kappa_{\mathrm{latt}} = \kappa_i \left(\frac{\omega_0}{\omega_{\mathrm{M}}}\right) \arctan\left(\frac{\omega_{\mathrm{M}}}{\omega_0}\right) \tag{7}$$

with

$$\left(\frac{\omega_0}{\omega_{\mathrm{M}}}\right)^2 = \frac{\chi T}{C(1-C)}, \tag{8}$$

where ω_{M} is the phonon frequency corresponding to the maximum of the acoustic branch of the phonon spectrum, ω_0 is the phonon frequency where the intrinsic mean free path is equal to that due to solute atoms, χ is a constant, and C is the concentration of the solute atoms. In the case of the MgO–FeO system, κ_i is the solid-solution thermal conductivity without the solute-atom phonon scattering and is given by:

$$\kappa_i = C\kappa_{\mathrm{MgO}} + (1-C)\kappa_{\mathrm{FeO}}. \tag{9}$$

On the κ_{latt} versus composition plot (Fig. 3), we fit Eq. (7) with room-temperature Fp conductivity data and obtained the χ value as 1.8×10^{-6} K^{-1}. The fitting result predicts substantially strong impurity scattering in the MgO–FeO system and the lowest thermal conductivity at $(Mg_{0.08}Fe_{0.92})O$ composition. We then estimate the κ_{latt} of (Mg, Fe)O at 900 and 1500 K. Those of MgO and $Fe_{1-x}O$ end-members are from the literature (Touloukian et al., 1970; Akiyama et al., 1992). The chemical composition showing the minimum thermal conductivity shifts to the $(Mg_{0.30}Fe_{0.70})O$ composition at high temperature.

3.3. The effect of iron spin crossover on lattice thermal conductivity of (Mg, Fe)O Fp

We observed an anomalous pressure response of the κ_{latt} of $(Mg_{0.81}Fe_{0.19})O$ Fp, which is likely due to the consequence of iron spin crossover (Fig. 2). The damped harmonic oscillator–phonon gas model predicts the pressure dependence of κ_{latt} of minerals:

$$\frac{\partial(\ln \kappa_{\mathrm{latt}})}{\partial P} = \frac{1}{K_{\mathrm{T}}}\left(4\gamma + \frac{1}{3}\right), \tag{10}$$

where K_{T} is the isothermal bulk modulus and γ is the Grüneisen parameter (Hofmeister, 1999). This model with thermoelastic parameters of MgO (Tange et al., 2009) agrees with the high-pressure κ_{latt} of MgO periclase measured by Dalton et al. (2013) (Fig. 4). In the same manner, we calculated the pressure dependence of κ_{latt} of $(Mg_{0.81}Fe_{0.19})O$ Fp both in high-spin and low-spin states from the model expressed by Eq. (10) and proposed thermoelastic parameters of high- and low-spin Fp (Speziale et al., 2007). The conductivity profile for high-spin Fp given by a red curve in Fig. 4 is in good agreement with our data up to 30 GPa, but deviates at higher pressures. The pressure where the conductivity begins to decrease matches the pressure for the onset of mixed spin state, in which high-spin and low-spin irons coexist in variable fractions in $(Mg_{0.81}Fe_{0.19})O$ (Tsuchiya et al., 2006). Within such a mixed spin region, Fp can be regarded as three component mixtures of MgO, high-spin FeO, and low-spin FeO. FeO in a different spin state acts as an additional phonon scatterer and hence lowers κ_{latt}. Compression experiments revealed the low-spin Fp is less compressible than the high-spin Fp (Lin et al., 2013), indicating that, based on Eq. (10), the pressure dependence of the κ_{latt} of low-spin Fp is smaller than that in the high-spin state. A combination of our low-spin Fp data and the damped harmonic oscillator–phonon gas model yields $\kappa_{\mathrm{latt}} = 13.5 \pm 2.2$ W/m/K at 135 GPa and 300 K; significantly lower than 377 W/m/K of MgO periclase at identical conditions (Fig. 4).

The iron spin crossover occurs in a broader pressure range at high temperatures of the Earth's lower mantle (Tsuchiya et al., 2006). The effect of the spin crossover on the κ_{latt} of Fp should therefore be diluted in the lower mantle in comparison to what was observed at room temperature in this study.

3.4. Electrical conductivity of $(Mg_{0.81}Fe_{0.19})O$ Fp at high P–T conditions

The computation of the electronic density of states of $(Mg_{0.75}Fe_{0.25})O$ Fp suggested an insulator–metal transition above 5 GPa and 2000 K, and predicted its electrical conductivity to be as high as $4.0 \pm 0.4 \times 10^4$ S/m at 136 GPa and 4000 K (Holmström and Stixrude, 2015). In order to verify such a large electronic contribution to the Fp conductivity at CMB conditions, we measured the electrical conductivity of $(Mg_{0.81}Fe_{0.19})O$ Fp up to 140 GPa and 2730 K. The *P–T* conditions of the experiments are shown in Fig. 5, considering a fraction of low-spin iron in $(Mg_{0.81}Fe_{0.19})O$ proposed by Tsuchiya et al. (2006). We first carried out an experiment at 22 GPa up to 1710 K, where iron is high-spin in Fp. The data obtained show an insulating behavior of the sample (i.e., increasing electrical conductivity with increasing temperature), consistent with those for $(Mg_{0.80}Fe_{0.20})O$ Fp with $Fe^{3+}/(Fe^{3+} + Fe^{2+}) = 0.04$ that is very similar chemical composition to our sample at 10 GPa measured by Dobson and Brodholt (2000) (Fig. 6). We then compressed the same Fp sample to 63, 116, and 131 GPa, and measured its high-temperature electrical conductivity at each pressure. Our measurements revealed that $(Mg_{0.81}Fe_{0.19})O$ Fp remains an insulator up to 140 GPa and 2730 K (Figs. 5 and 6). Even if we take temperature dependence into account, the obtained electrical conductivity of $(Mg_{0.81}Fe_{0.19})O$ Fp is much lower than the computed conductivity value of $4.0 \pm 0.4 \times 10^4$ S/m at CMB conditions (Holmström and Stixrude, 2015) (Fig. 6), indicating a negligible contribution of the electronic term to total thermal conductivity of Fp in the Earth's lower mantle conditions.

4. Geophysical implications

4.1. Thermal conductivity of Fp at CMB

Here we estimate the thermal conductivity of (Mg, Fe)O Fp at CMB conditions, considering overall thermal conduction mechanisms (κ_{latt}, κ_{rad}, and κ_{el}). The CMB temperature is assumed to be

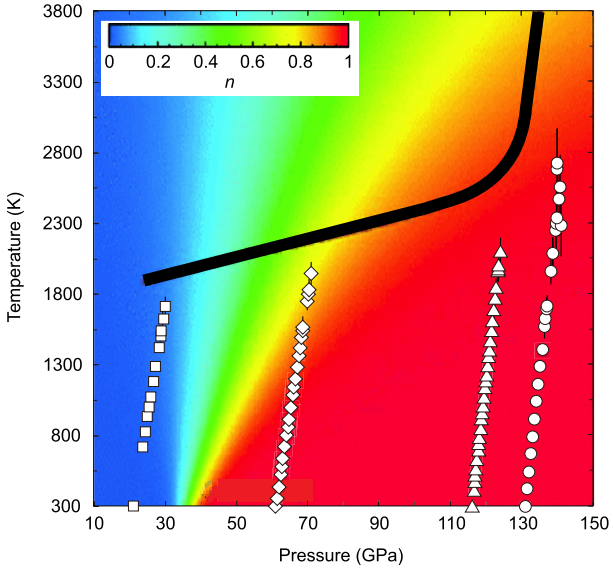

Fig. 5. *P–T* conditions of the electrical conductivity measurements on $(Mg_{0.81}Fe_{0.19})O$ Fp (open symbols). Color contour shows fraction of low-spin iron in $(Mg_{0.81}Fe_{0.19})O$ Fp (Tsuchiya et al., 2006). The black line is a typical lower mantle geotherm. (For interpretation of the references to color in this figure legend, the reader is referred to the web version of this article.)

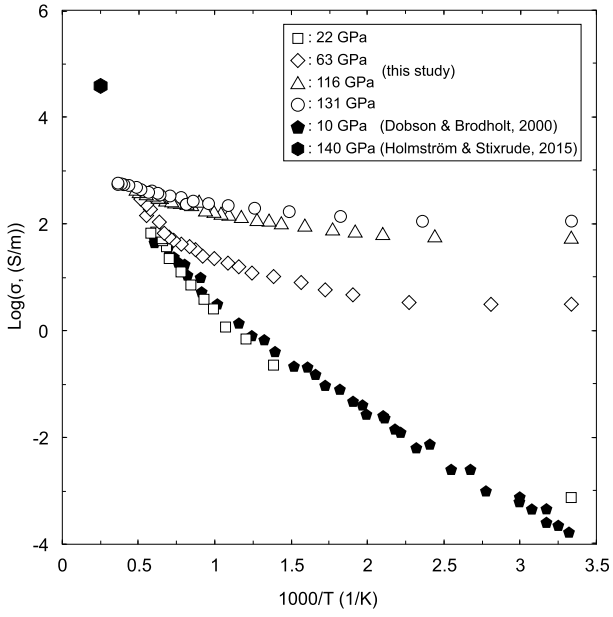

Fig. 6. Electrical conductivity (σ) of Fp as a function of reciprocal temperature. Open symbols indicate high *P–T* electrical conductivity of $(Mg_{0.81}Fe_{0.19})O$ Fp with $Fe^{3+}/(Fe^{3+} + Fe^{2+}) = 0.049 \pm 0.017$ obtained in this study. Pentagon-shaped symbols show the electrical conductivity of $(Mg_{0.80}Fe_{0.20})O$ Fp with $Fe^{3+}/(Fe^{3+} + Fe^{2+}) = 0.04$ at 10 GPa (Dobson and Brodholt, 2000). Hexagon symbol is the computed σ_{el} of $(Mg_{0.75}Fe_{0.25})O$ Fp at 136 GPa and 4000 K (Holmström and Stixrude, 2015). Pressures shown in the figure are determined at 300 K.

3700 K; the same as in our previous study (Ohta et al., 2012a). We first consider the temperature effect on the κ_{latt} of Fp at 135 GPa. Present results showed that the κ_{latt} of low-spin $(Mg_{0.81}Fe_{0.19})O$ Fp is 13.5 ± 2.2 W/m/K at 135 GPa and 300 K (Fig. 4). In a pure simple crystal, temperature dependence of the κ_{latt} typically follows T^{-1} relation, while point defect, mass disorder, and other imperfections in the crystal make the temperature dependence weaker. Manthilake et al. (2011) found that thermal conductivity of $(Mg_{0.95}Fe_{0.05})O$ and $(Mg_{0.80}Fe_{0.20})O$ Fp showed $T^{-0.24}$ dependence at 8 and 14 GPa. Here we apply the same temperature

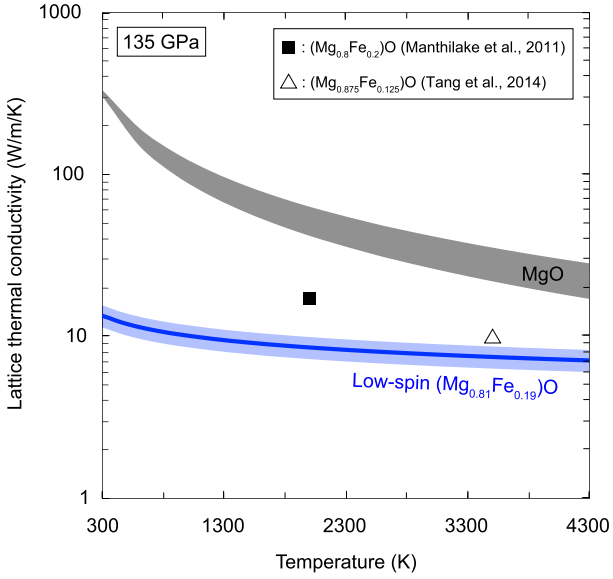

Fig. 7. Temperature dependence of κ_{latt} of $(Mg_{0.81}Fe_{0.19})O$ Fp at 135 GPa. Blue line indicates temperature response of κ_{latt} of low-spin $(Mg_{0.81}Fe_{0.19})O$ Fp at 135 GPa based on $T^{-0.24}$ relation proposed by Manthilake et al. (2011). Gray band shows κ_{latt} of MgO periclase at 135 GPa from experiments and theoretical calculations (de Koker, 2010; Stackhouse et al., 2010; Tang and Dong, 2010; Manthilake et al., 2011). Square, thermal conductivity of $(Mg_{0.8}Fe_{0.2})O$ at 135 GPa and 2000 K (Manthilake et al., 2011); triangle, low-spin $(Mg_{0.875}Fe_{0.125})O$ at 135 GPa and 3500 K (Tang et al., 2014). (For interpretation of the references to color in this figure legend, the reader is referred to the web version of this article.)

dependence to our low-spin Fp (Fig. 7). The $T^{-0.24}$ relation yields 7.4 ± 1.2 W/m/K at the CMB (135 GPa and 3700 K), which is $65 \sim 78\%$ lower than the κ_{latt} of MgO at identical *P–T* conditions (de Koker, 2010; Stackhouse et al., 2010; Tang and Dong, 2010; Manthilake et al., 2011). Our estimate of the conductivity shows a value lower than the κ_{latt} of $(Mg_{0.80}Fe_{0.20})O$ Fp reported by Manthilake et al. (2011), even when the same $T^{-0.24}$ relation is employed. The difference is mainly derived from the reduced κ_{latt} because of the iron spin crossover. Tang et al. (2014) computed the κ_{latt} of (Mg, Fe)O Fp containing 12.5 mol% low-spin iron, which is in good agreement with our result in light of the difference in iron concentration.

According to the optical absorption measurements, Fp shows low κ_{rad} relative to Bdg and slightly reduced κ_{rad} across the spin crossover (Goncharov et al., 2006; Keppler et al., 2007; Kavner and Rainey, 2016). Lobanov et al. (2016) revisited the high-pressure absorption coefficient for $(Mg_{0.85}Fe_{0.15})O$ Fp (Goncharov et al., 2006) and calculated the κ_{rad} to be 0.2 W/m/K at the bottom of the mantle taking into account temperature effect on its optical absorption spectra. Therefore, we conclude that the role of radiative heat transfer in low spin Fp is negligible at deep lower mantle conditions. The present electrical conductivity measurements on $(Mg_{0.81}Fe_{0.19})O$ Fp show its insulating behavior up to the lowermost mantle *P–T* conditions and electrical conductivity about two orders of magnitude lower than the computational prediction by Holmström and Stixrude (2015) (Fig. 6). Consequently, the lattice thermal conduction is primarily in Fp, and κ_{rad} and κ_{el} are vanishingly small relative to κ_{latt}, even at high temperatures in the Earth's lowermost mantle.

4.2. Inference of thermal conductivity of Fe- and Al-bearing Bdg and PPv

We previously carried out κ_{latt} measurements on $MgSiO_3$ Bdg and post-perovskite (PPv) up to 144 GPa, and estimated the values at CMB conditions to be 9 W/m/K for Bdg and 11 W/m/K

for PPv (Ohta et al., 2012a). However, both iron and aluminum impurities in Bdg reduce its κ_{latt} as observed for other rock-forming minerals. Manthilake et al. (2011) first demonstrated that the incorporation of 3 mol% iron and 2 mol% aluminum diminished the thermal conductivity of Bdg by ~75% at 26 GPa and 300 K. However, such strong impurity effects for Bdg were not confirmed by more recent studies. Ohta et al. (2014b) reported a negligible effect of 2 wt.% Al_2O_3 incorporation into Bdg on its κ_{latt}. Theoretical calculations made on the basis of scaling relations predict that the 10 mol% iron impurity reduces only 10% of the κ_{latt} of Bdg (Ammann et al., 2014; Stackhouse et al., 2015). These recent reports argued that a strong impurity effect on the κ_{latt} of Bdg is unlikely to occur. $MgSiO_3$ PPv showed ~60% higher κ_{latt} than Bdg, but iron substitution in PPv could induce the same degree of conductivity reduction (Ohta et al., 2012a; Ammann et al., 2014). Thus, iron-bearing PPv is likely to show similar conductivity to that of Bdg. We can expect that the influence of the spin crossover on the κ_{latt} of Bdg is much weaker than in Fp because of the lower iron content and the smaller spin crossover effect on the elastic properties of Bdg relative to Fp (Lin et al., 2013).

The value of the κ_{rad} of Bdg strongly depends on the iron content and its valence state. The κ_{rad} of $(Mg_{0.9}Fe_{0.1})SiO_3$ Bdg with ~10% of $Fe^{3+}/(Fe^{3+} + Fe^{2+})$ ratio was estimated to be around 2 W/m/K at CMB conditions, while that with ~40% of the total iron in the Fe^{3+} state showed higher value of about 6 W/m/K (Goncharov et al., 2015; Kavner and Rainey, 2016). A recent report by Lobanov et al. (2016) shows the κ_{rad} of $(Mg_{0.9}Fe_{0.1})SiO_3$ Bdg and PPv are 2.2 and 1.2 W/m/K at 135 GPa and 4000 K, respectively. How large is the contribution of electronic conduction in Bdg and PPv? The electrical conductivity measurements on Bdg have been performed, and small-polaron or ionic conduction was found to be dominant at deep lower mantle conditions (Ohta et al., 2008; Sinmyo et al., 2014). These results indicate a very minor contribution of electronic conduction for Bdg. Although PPv shows electrical conductivity a few orders of magnitude higher than Bdg, the measured conductivity of $\sim 10^2$ S/m is too low to contribute as electronic thermal conduction (Ohta et al., 2008).

4.3. *Thermal conductivity of the lowermost mantle and its influence on core and mantle dynamics*

We consider the potential importance of thermal conductivity of (Mg, Fe)O Fp in the bulk thermal conductivity of the lower mantle rocks. The thermal conductivity of Bdg + Fp mixture at the CMB is calculated using the Hashin–Shtrikman averaging. The parallel and series models are also employed to calculate the thermal conductivity of a composite with a layering structure. We assume the κ_{latt} of $(Mg_{0.9}Fe_{0.1})SiO_3$ Bdg is 8.1 W/m/K at CMB conditions, 10% lower than that of $MgSiO_3$ Bdg, based on recent theoretical calculations (Ammann et al., 2014; Stackhouse et al., 2015). As we discussed above, iron-bearing PPv would show similar κ_{latt} to that of Bdg. We first calculated the κ_{latt} of a pyrolitic lowermost mantle, a mixture of 80 vol% $(Mg_{0.90}Fe_{0.10})SiO_3$ Bdg + 20 vol% $(Mg_{0.81}Fe_{0.19})O$ Fp, to be 7.9 ± 1.3 W/m/K (Fig. 8a), which is lower than the ~11 W/m/K for an iron-free mixture (gray band in Fig. 8). Such ~40% difference is mainly derived from the strongly reduced κ_{latt} of Fp due to the iron substitution and the effect of spin crossover. In the iron-free system, the bulk thermal conductivity is sensitive to MgO content and to the layering structure of these two minerals because of the much higher thermal conductivity of MgO than that of $MgSiO_3$ Bdg (black lines in Fig. 8a). On the other hand, iron incorporation into these two minerals makes the lattice conductivity similar, indicating less variation in lower mantle κ_{latt} caused by the difference in the proportion (i.e., Mg/Si ratio) and texture of Bdg and Fp (blue lines in Fig. 8a).

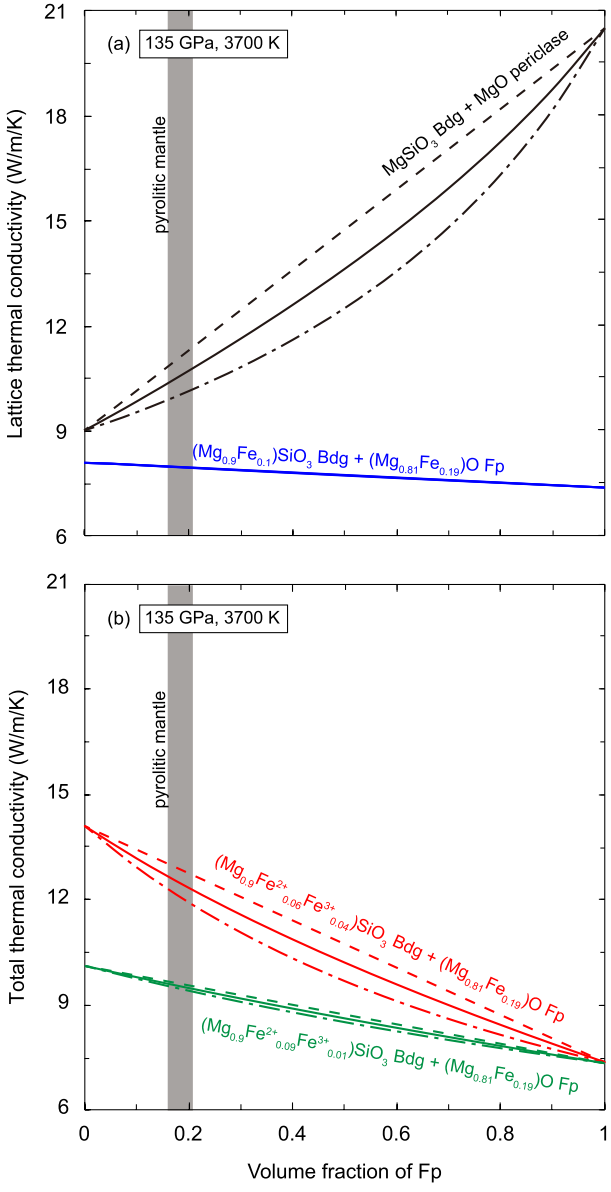

Fig. 8. (a) Lattice thermal conductivities of the mixture of $(Mg_{0.9}Fe_{0.1})SiO_3$ Bdg and $(Mg_{0.81}Fe_{0.19})O$ Fp (blue lines) and the mixture of $MgSiO_3$ Bdg and MgO periclase (black lines) as function of (Mg, Fe)O content. The results for an iron-free system are taken from our previous study (Ohta et al., 2012a). (b) Total thermal conductivities of the mixture of $(Mg_{0.9}Fe^{2+}_{0.06}Fe^{3+}_{0.04})SiO_3$ Bdg and $(Mg_{0.81}Fe_{0.19})O$ Fp (red lines) and the mixture of $(Mg_{0.9}Fe^{2+}_{0.09}Fe^{3+}_{0.01})SiO_3$ Bdg and $(Mg_{0.81}Fe_{0.19})O$ Fp (green lines) as function of (Mg, Fe)O content. *P–T* condition is set to be 135 GPa and 3700 K. Gray bands indicate volume fraction of these minerals in pyrolite composition. Lines indicate several effective media models for conductivity of the two-phase mixture. Broken line, parallel model; chain line, series model; solid line, Hashin–Shtrikman average. (For interpretation of the references to color in this figure legend, the reader is referred to the web version of this article.)

Then we consider total thermal conductivity of a pyrolitic lowermost mantle. The lattice thermal conduction is primarily in Fp, and κ_{rad} and κ_{el} are vanishingly small even at the Earth's lowermost mantle. Conversely, the reported κ_{rad} of $(Mg_{0.9}Fe_{0.1})SiO_3$ Bdg ranges from about 2 to 6 W/m/K depending on its $Fe^{3+}/(Fe^{3+} + Fe^{2+})$ ratio (Goncharov et al., 2015), and the κ_{el} of Bdg can be ignored (Ohta et al., 2008; Sinmyo et al., 2014). Considering all these thermal conduction mechanism, we computed bulk total thermal conductivity of $(Mg_{0.9}Fe_{0.1})SiO_3$ Bdg and $(Mg_{0.81}Fe_{0.19})O$ Fp aggregate at 135 GPa and 3700 K (Fig. 8b). Interestingly, in the iron-bearing system, Bdg turns out to be much better heat conductor than Fp in contrast to the iron-free system. As a re-

sult, the thermal conductivity of pyrolitic mantle ranges between 9.4 and 12.8 W/m/K at the CMB condition (gray band in Fig. 8b). PPv-dominant pyrolitic mantle would show the similar conductivity value considering iron substitution effect on its κ_{latt} (Ammann et al., 2014), moderate value of its κ_{rad} at the CMB condition (Lobanov et al., 2016), and negligible contribution of its κ_{el} (Ohta et al., 2008).

The conductive heat flux from the core to mantle (Q_{CMB}) can be estimated based on Fourier's heat law:

$$Q_{\mathrm{CMB}} = A_{\mathrm{CMB}} \kappa_{\mathrm{LM}} \frac{dT}{dz}, \tag{11}$$

where A_{CMB}, κ_{LM} and dT/dz are the surface area of the CMB, the lower mantle thermal conductivity and the temperature gradient in a mantle thermal boundary layer, respectively. The κ_{LM} has been traditionally assumed to be 10 W/m/K (Stacey, 1992). The often-used κ_{LM} and temperature profiles at the lowermost mantle inferred from seismology and mineral physics imply a Q_{CMB} ~15 TW (Lay et al., 2006; van der Hilst et al., 2007). Since our new estimate of the pyrolitic lowermost mantle thermal conductivity ranging from 9.4 to 12.8 W/m/K is consistent with the traditional value, it still supports the view of a high CMB heat flow inferred from seismology (Lay et al., 2006; van der Hilst et al., 2007). The present-day global average heat flux at the CMB exceeding 9 TW is sufficient to drive the present-day geodynamo by thermochemical convection and implies a very young inner core (Olson, 2016).

The evidence for laterally heterogeneous CMB heat flux also came from the seismological observations (Lay et al., 2006, 2008; van der Hilst et al., 2007). The CMB heat flux heterogeneity is partially derived from lower mantle thermal conductivity heterogeneity due to temperature and chemical variations in the lower mantle, which provides a bottom-up control on the mantle convection style (Ammann et al., 2014) and a top-down control of core dynamics (Sumita and Olson, 1999; Olson, 2016). The difference in iron impurity effect on κ_{latt} between Fp and Bdg implies the importance of iron partitioning between these two minerals for the κ_{latt} of the lower mantle (Fig. 8a). The iron partitioning between Fp and Bdg (or PPv) changes with pressure, temperature, ferric iron content (i.e., oxygen fugacity), and spin state (e.g., Sinmyo et al., 2008; Irifune et al., 2010; Piet et al., 2016). Distribution of iron among the lower mantle minerals and ferric iron content in Bdg also change significance of radiative thermal conduction in Bdg at high temperature conditions, and thus vary total thermal conductivity of pyrolitic lowermost mantle (Fig. 8b).

It has been repeatedly argued that FeO-rich rocks might accumulate above the CMB by various processes and cause the ultra low velocity zones (ULVZs) (e.g., Dobson and Brodholt, 2005). Iron-rich (Mg, Fe)O magnesiowüstite shows lower κ_{latt} than Fp due to higher iron content (Fig. 3), but could exhibit high electronic thermal conduction due to metallization. Significant electron conduction has been confirmed on $Fe_{0.96}O$ wüstite and $(Mg_{0.20}Fe_{0.80})O$ and $(Mg_{0.05}Fe_{0.95})O$ magnesiowüstite at deep lower mantle conditions by means of high P–T electrical conductivity measurements (Ohta et al., 2012b, 2014a). The electrical conductivity of metallic $Fe_{0.96}O$ wüstite was obtained to be 9×10^4 S/m, corresponding to $\kappa_{\mathrm{el}} = 8.1$ W/m/K, at 135 GPa and 4000 K, and iron-rich magnesiowüstites also showed similar electrical conductivity under such CMB conditions. Therefore, the total thermal conductivity of iron-rich magnesiowüstite and wüstite may reach about 10 W/m/K near the base of the mantle, but it differs little from that of the pyrolitic mantle estimated in this study. Balance among κ_{latt}, κ_{rad} and κ_{el} in each lower mantle mineral is likely to prevent occurrence of the region with extremely high thermal conductivity at the base of mantle.

5. Conclusions

We report the results of κ_{latt} measurements on $(Mg_{0.81}Fe_{0.19})O$ Fp up to 111 GPa and 300 K in a DAC. Results demonstrate a strong iron impurity effect of reducing the thermal conductivity. The κ_{latt} was further diminished during the iron spin crossover that occurred between 30 and 55 GPa. We also measured the electrical conductivity of an identical Fp sample up to 140 GPa and 2730 K. Our study confirmed the insulating behavior of Fp throughout the experiments. Therefore, we conclude that the κ_{el} of Fp is negligible at lower mantle conditions. Our finding of a strong iron impurity effect on the κ_{latt} of (Mg, Fe)O relative to that of Bdg indicates that iron partitioning between these two minerals remarkably affects the bulk thermal conductivity of the lower mantle as well as the effect of ferric iron content on κ_{rad} of Bdg. The total thermal conductivity of a pyrolitic lower mantle ranges between 9.4 and 12.8 W/m/K at the CMB, depending on the magnitude of κ_{rad} of Bdg. These results indicate that the distribution of iron and its valence state in the lower mantle minerals are important factors to control the thermal conductivity and thermal structure of the Earth's lower mantle.

Acknowledgements

Ookayama Materials Analysis Division at Tokyo Institute of Technology helped the estimate of $Fe^{3+}/(Fe^{3+} + Fe^{2+})$ ratio in our Fp sample. High-pressure and high-temperature electrical conductivity experiments were performed at BL10XU, SPring-8 (proposal number 2016B0080). Comments from two anonymous reviewers helped to improve the manuscript. This work was supported by JSPS KAKENHI Grant Number JP15H05827.

References

Akahama, Y., Kawamura, H., 2006. Pressure calibration of diamond anvil Raman gauge to 310 GPa. J. Appl. Phys. 100, 043516.
Akiyama, T., Ohta, H., Takahashi, R., Waseda, Y., Yagi, J., 1992. Measurement and modeling of thermal conductivity for dense iron oxide and porous iron ore agglomerates in stepwise reduction. ISIJ Int. 32, 829–837.
Ammann, M., Walker, A., Stackhouse, S., Wookey, J., Forte, A., Brodholt, J., Dobson, D., 2014. Variation of thermal conductivity and heat flux at the Earth's core mantle boundary. Earth Planet. Sci. Lett. 390, 175–185.
Dalton, D.A., Hsieh, W.-P., Hohensee, G.T., Cahill, D.G., Goncharov, A.F., 2013. Effect of mass disorder on the lattice thermal conductivity of MgO periclase under pressure. Sci. Rep. 3, 2400.
de Koker, N., 2010. Thermal conductivity of MgO periclase at high pressure: implications for the D" region. Earth Planet. Sci. Lett. 292, 392–398.
Dobson, D.P., Cohen, N.S., Pankhurst, Q.A., Brodholt, J.P., 1998. A convenient method for measuring ferric iron in magnesiowüstite (MgO–$Fe_{1-x}O$). Am. Mineral. 83, 794–798.
Dobson, D.P., Brodholt, J.P., 2000. The electrical conductivity of the lower mantle phase magnesiowüstite at high temperatures and pressures. J. Geophys. Res. 105, 531–538.
Dobson, D.P., Brodholt, J.P., 2005. Subducted banded iron formations as a source of ultralow-velocity zones at the core–mantle boundary. Nature 434, 371–374.
Goncharov, A.F., Struzhkin, V.V., Jacobsen, S.D., 2006. Reduced radiative conductivity of low-spin (Mg, Fe)O in the lower mantle. Science 321, 1205–1208.
Goncharov, A., Lobanov, S., Tan, X., Hohensee, G., Cahill, D., Lin, J.-F., Thomas, S.-M., Okuchi, T., Tomioka, N., 2015. Experimental study of thermal conductivity at high pressures: Implications for the deep Earth's interior. Phys. Earth Planet. Inter. 247, 11–16.
Haigis, V., Salanne, M., Jahn, S., 2012. Thermal conductivity of MgO, $MgSiO_3$ perovskite and post-perovskite in the Earth's deep mantle. Earth Planet. Sci. Lett. 355–356, 102–108.
Ho, C., Powell, R., Liley, P., 1972. Thermal conductivity of the elements. J. Phys. Chem. Ref. Data 1, 279–421.
Hofmeister, A.M., 1999. Mantle values of thermal conductivity and the geotherm from phonon lifetimes. Science 283, 1699–1706.
Holmström, E., Stixrude, L., 2015. Spin crossover in ferropericlase from first-principles molecular dynamics. Phys. Rev. Lett. 114, 117202.
Imada, S., Ohta, K., Yagi, T., Hirose, K., Yoshida, H., Nagahara, H., 2014. Measurements of lattice thermal conductivity of MgO to core–mantle boundary pressures. Geophys. Res. Lett. 41, 4542–4547.

Irifune, T., Shinmei, T., McCammon, C.A., Miyajima, N., Rubie, D.C., Frost, D.J., 2010. Iron partitioning and density changes of pyrolite in Earth's lower mantle. Science 327, 193–195.
Kavner, A., Rainey, E., 2016. In: Deep Earth: Physics and Chemistry of the Lower Mantle and Core, pp. 31–42.
Keppler, H., Kantor, I., Dubrovinsky, L., 2007. Optical absorption spectra of ferropericlase to 84 GPa. Am. Mineral. 92, 433–436.
Komabayashi, T., Hirose, K., Nagaya, Y., Sugimura, E., Ohishi, Y., 2010. High-temperature compression of ferropericlase and the effect of temperature on iron spin transition. Earth Planet. Sci. Lett. 297, 691–699.
Lay, T., Hernlund, J., Garnero, E.J., Thorne, M.S., 2006. A post-perovskite lens and D" heat flux beneath the central Pacific. Science 314, 1272–1276.
Lay, T., Hernlund, J., Buffett, B., 2008. Core–mantle boundary heat flow. Nat. Geosci. 1, 25–32.
Lin, J.-F., Speziale, S., Mao, Z., Marquardt, H., 2013. Effects of the electronic spin transitions of iron in lower mantle minerals: implications for deep mantle geophysics and geochemistry. Rev. Geophys. 51, 244–275.
Lobanov, S., Holtgrewe, N., Goncharov, A., Lin, J.-F., 2016. Radiative conductivity and abundance of post-perovskite in the lowermost mantle. arXiv:1609.06996.
Manthilake, G.M., de Koker, N., Frost, D.J., McCammon, C.A., 2011. Lattice thermal conductivity of lower mantle minerals and heat flux from Earth's core. Proc. Natl. Acad. Sci. USA 108, 17901–17904.
Morton, I.P., Lewis, M.F., 1971. Effect of iron impurities on the thermal conductivity of magnesium oxide single crystals below room temperature. Phys. Rev. B 3, 552–559.
Ohta, K., Onoda, S., Hirose, K., Sinmyo, R., Shimizu, K., Sata, N., Ohishi, Y., Yasuhara, A., 2008. The electrical conductivity of post-perovskite in Earth's D" layer. Science 320, 89–91.
Ohta, K., Yagi, T., Taketoshi, N., Hirose, K., Komabayashi, T., Baba, T., Ohishi, Y., Hernlund, J., 2012a. Lattice thermal conductivity of $MgSiO_3$ perovskite and post-perovskite at the core–mantle boundary. Earth Planet. Sci. Lett. 349–350, 109–115.
Ohta, K., Cohen, R.E., Hirose, K., Haule, K., Shimizu, K., Ohishi, Y., 2012b. Experimental and theoretical evidence for pressure-induced metallization in FeO with rocksalt-type structure. Phys. Rev. Lett. 108, 026403.
Ohta, K., Fujino, K., Kuwayama, Y., Kondo, T., Shimizu, K., Ohishi, Y., 2014a. Highly conductive iron-rich (Mg,Fe)O magnesiowüstite and its stability in the Earth's lower mantle. J. Geophys. Res. 119, 4656–4665.
Ohta, K., Yagi, T., Hirose, K., 2014b. Thermal diffusivities of $MgSiO_3$ and Al-bearing $MgSiO_3$ perovskites. Am. Mineral. 99, 94–97.
Olson, P., 2016. Mantle control of the geodynamo: consequences of top-down regulation. Geochem. Geophys. Geosyst. 17, 1935–1956.
Padture, N., Klemens, P., 1997. Low thermal conductivity in garnets. J. Am. Ceram. Soc. 80, 1018–1020.
Piet, H., Badro, J., Nabiei, F., Dennenwaldt, T., Shim, S.-H., Cantoni, M., Hébert, C., Gillet, P., 2016. Spin and valence dependence of iron partitioning in Earth's deep mantle. Proc. Natl. Acad. Sci. USA 113, 11127–11130.
Ross, R.G., Andersson, P., Sundqvist, B., Bäckström, G., 1984. Thermal conductivity of solids and liquids under pressure. Rep. Prog. Phys. 47, 1347–1402.
Sinmyo, R., Hirose, K., Nishio-Hamane, D., Seto, Y., Fujino, K., Sata, N., Ohishi, Y., 2008. Partitioning of iron between perovskite/postperovskite and ferropericlase in the lower mantle. J. Geophys. Res. 113, B11204.
Sinmyo, R., Pesce, G., Greenberg, E., McCammon, C., Dubrovinsky, L., 2014. Lower mantle electrical conductivity based on measurements of Al,Fe-bearing perovskite under lower mantle conditions. Earth Planet. Sci. Lett. 393, 165–172.
Smith, D., Fayette, S., Grandjean, S., Martin, C., Telle, R., Tonnessen, T., 2003. Thermal resistance of grain boundaries in alumina ceramics and refractories. J. Am. Ceram. Soc. 86, 105–111.
Speziale, S., Lee, V.E., Clark, S.M., Lin, J.-F., Pasternak, M.P., Jeanloz, R., 2007. Effects of Fe spin transition on the elasticity of (Mg,Fe)O magnesiowüstites and implications for the seismological properties of the Earth's lower mantle. J. Geophys. Res. 112, B10212.
Stackhouse, S., Stixrude, L., Karki, B., 2010. Thermal conductivity of periclase (MgO) from first principles. Phys. Rev. Lett. 104, 208501.
Stackhouse, S., Stixrude, L., Karki, B., 2015. First-principles calculations of the lattice thermal conductivity of the lower mantle. Earth Planet. Sci. Lett. 427, 11–17.
Stacey, F., 1992. Physics of the Earth, 3rd ed. Brookfield, Brisbane, Australia.
Sumita, I., Olson, P., 1999. A Laboratory model for convection in Earth's core driven by a thermally heterogeneous mantle. Science 286, 1547–1549.
Tang, X., Dong, J., 2010. Lattice thermal conductivity of MgO at conditions of Earth's interior. Proc. Natl. Acad. Sci. USA 107, 4539–4543.
Tang, X., Ntam, M., Dong, J., Rainey, E., Kavner, A., 2014. The thermal conductivity of Earth's lower mantle. Geophys. Res. Lett. 41, 2746–2752.
Tange, Y., Nishihara, Y., Tsuchiya, T., 2009. Unified analyses for *P–V–T* equation of state of MgO: A solution for pressure-scale problems in high *P–T* experiments. J. Geophys. Res. 114, B03208.
Touloukian, Y.S., Powell, R.W., Ho, C.Y., Klemens, P.G., 1970. Thermal conductivity nonmetallic solids. In: Thermophysical Properties of Matter, vol. 2. Thermophys. Prop. Res. Cent., New York.
Tsuchiya, T., 2003. First-principles prediction of the *P–V–T* equation of state of gold and the 660-km discontinuity in Earth's mantle. J. Geophys. Res. 108, 2462.
Tsuchiya, T., Wentzcovitch, R.M., da Silva, C.R., de Gironcoli, S., 2006. Spin transition in magnesiowüstite in Earth's lower mantle. Phys. Rev. Lett. 96, 198501.
van der Hilst, R.D., de Hoop, M.V., Wang, P., Shim, S.-H., Ma, P., Tenorio, L., 2007. Seismostratigraphy and thermal structure of Earth's core–mantle boundary region. Science 315, 1813–1817.
Yagi, T., Ohta, K., Kobayashi, K., Taketoshi, N., Hirose, K., Baba, T., 2011. Thermal diffusivity measurement in a diamond anvil cell using a light pulse thermoreflectance technique. Meas. Sci. Technol. 22, 024011.